Large loss of CO_2 in winter observed across pan-arctic permafrost region

Authors: Susan. M. Natali[1*]†, Jennifer D. Watts[1]†, Brendan M. Rogers[1], Stefano Potter[1], Sarah M. Ludwig[1], Anne-Katrin Selbmann[2], Patrick F. Sullivan[3], Benjamin W. Abbott[4], Kyle A. Arndt[5], Leah Birch[1], Mats P. Björkman[6], A. Anthony Bloom[7], Gerardo Celis[8], Torben R. Christensen[9], Casper T. Christiansen[10], Roisin Commane[11], Elisabeth J. Cooper[12], Patrick Crill[13], Claudia Czimczik[14], Sergey Davydov[15], Jinyang Du[16], Jocelyn E. Egan[17], Bo Elberling[18], Eugenie S. Euskirchen[19], Thomas Friborg[20], Hélène Genet[19], Mathias Göckede[21], Jordan P. Goodrich[5,22], Paul Grogan[23], Manuel Helbig[24], Elchin E. Jafarov[25], Julie D. Jastrow[26], Aram A. M. Kalhori[5], Yongwon Kim[27], John Kimball[16], Lars Kutzbach[28], Mark J. Lara[29], Klaus S. Larsen[20], Bang-Yong Lee[30], Zhihua Liu[16], Michael M. Loranty[31], Magnus Lund[9], Massimo Lupascu[32], Nima Madani[7], Avni Malhotra[33], Roser Matamala[26], Jack McFarland[34], A. David McGuire[19], Anders Michelsen[35], Christina Minions[1], Walter C. Oechel[5,36], David Olefeldt[37], Frans-Jan W. Parmentier[38, 39], Norbert Pirk[40], Ben Poulter[41], William Quinton[42], Fereidoun Rezanezhad[43], David Risk[44], Torsten Sachs[45], Kevin Schaefer[46], Niels M. Schmidt[47], Edward A.G. Schuur[8], Philipp R. Semenchuk[48], Gaius Shaver[49], Oliver Sonnentag[50], Gregory Starr[51], Claire C. Treat[52], Mark P. Waldrop[34], Yihui Wang[5], Jeffrey Welker[53,54], Christian Wille[45], Xiaofeng Xu[5], Zhen Zhang[55], Qianlai Zhuang[56], Donatella Zona[5,57]

Affiliations:

[1] Woods Hole Research Center, Falmouth, MA 02540, USA.
[2] University of Bayreuth, Bayreuth, Germany.
[3] Environment and Natural Resources Institute, University of Alaska, Anchorage, AK 99508. USA.
[4] Brigham Young University, Department of Plant and Wildlife Sciences, Provo, UT 84062, USA.
[5] Department of Biology, San Diego State University, San Diego, CA 92182, USA.
[6] Department of Earth Sciences, University of Gothenburg, PO Box 460, SE-405 30 Göteborg, Sweden.
[7] Jet Propulsion Laboratory, California Institute of Technology, Pasadena, CA 91109, USA.
[8] Center for Ecosystem Science and Society, Northern Arizona University, Flagstaff, AZ 86001, USA.
[9] Department of Bioscience, Arctic Research Centre, Aarhus University, Frederiksborgvej 399, 4000 Roskilde, Denmark.
[10] NORCE Norwegian Research Centre, Bjerknes Centre for Climate Research, Bergen, Norway.
[11] Dept. of Earth & Environmental Sciences, Columbia University, NY 10027, USA.
[12] Department of Arctic and Marine Biology, Faculty of Biosciences, Fisheries and Economics, UiT. The Arctic University of Norway, N9037 Tromsø, Norway.
[13] Dept. of Geological Sciences and Bolin Centre for Climate Research, Stockholm University, Sweden.
[14] Earth System Science, University of California, Irvine, CA 92697, USA.
[15] Northeast Science Station, Pacific Geographical Institute, Cherskii, Russia.
[16] Numerical Terradynamic Simulation Group, W.A. Franke College of Forestry & Conservation, University of Montana, Missoula, MT 59812, USA.
[17] Department of Earth Sciences, Dalhousie University, Halifax, NS, Canada.

[18] Center for Permafrost (CENPERM), Department of Geosciences and Natural Resource Management, University of Copenhagen, Øster Voldgade 10, DK-1350 Copenhagen, Denmark.
[19] University of Alaska Fairbanks, Institute of Arctic Biology, Fairbanks, AK 99775, USA.
[20] Department of Geosciences and Natural Resource Management, University of Copenhagen, Denmark.
[21] Max Planck Institute for Biogeochemistry, Jena, Germany.
[22] Scripps Institution of Oceanography, UCSD, La Jolla, CA 92037, USA.
[23] Department of Biology, Queen's University, Kingston, ON, Canada.
[24] McMaster University, School of Geography and Earth Sciences, Hamilton, ON, L8S 4K1.
[25] Los Alamos National Laboratory, New Mexico 87545, USA.
[26] Environmental Science Division, Argonne National Laboratory, Argonne, IL 60439, USA.
[27] International Arctic Research Center, University of Alaska Fairbanks, AK 99775, USA.
[28] Institute of Soil Science, Universät Hamburg, Hamburg, Germany.
[29] Department of Plant Biology, University of Illinois, Urbana, IL 61801, USA.
[30] Korea Polar Research Institute (KOPRI), Incheon 21990, Republic of Korea)
[31] Department of Geography, Colgate University, Hamilton, NY 13346, USA.
[32] Department of Geography, National University of Singapore, Singapore.
[33] Environmental Sciences Division and Climate Change Science Institute, Oak Ridge National Laboratory, Oak Ridge, TN 37831, USA.
[34] Geology, Minerals, Energy, and Geophysics Science Center, U.S. Geological Survey, Menlo Park, CA 94025, USA.
[35] Department of Biology, University of Copenhagen, Denmark.
[36] University of Exeter, Exeter, UK.
[37] University of Alberta, Department of Renewable Resources, Edmonton, Alberta, Canada.
[38] Department of Geosciences, University of Oslo, Oslo, Norway.
[39] Department of Physical Geography and Ecosystem Science, Lund University, Lund, Sweden.
[40] Department of Physical Geography and Ecosystem Science, Lund University, Sölvegatan 12, 22362 Lund, Sweden.
[41] NASA GSFC, Biospheric Sciences Lab., Greenbelt, MD 20771, USA.
[42] Wilfrid Laurier University, Waterloo, Ontario, Canada.
[43] Ecohydrology Research Group, Water Institute and Department of Earth & Environmental Sciences, University of Waterloo, 200 University Avenue West, Waterloo, ON, N2L 3G1, Canada.
[44] St. Francis Xavier University, Antigonish, Nova Scotia, Canada.
[45] GFZ German Research Centre for Geosciences, Telegrafenberg, Potsdam, Germany.
[46] National Snow and Ice Data Center, Boulder, CO 80309, USA.
[47] Arctic Research Centre, Department of Bioscience, Aarhus University, Roskilde, Denmark.
[48] Division of Conservation Biology, Vegetation Ecology and Landscape Ecology, Department of Botany and Biodiversity Research, Rennweg 14, 1030 Vienna, Austria.
[49] The Ecosystems Center, Marine Biological Laboratory, Woods Hole, MA 02543, USA.
[50] Université de Montréal, Département de géographie & Centre d'études nordiques, 520 chemin de la Côte Sainte Catherine, Montréal, QC H2V 2B8.
[51] Department of Biological Sciences, University of Alabama, Tuscaloosa, AL 35487, USA.
[52] Department of Environmental and Biological Science, University of Eastern Finland, Finland.
[53] Department of Biological Sciences, University of Alaska Anchorage, Anchorage, AK 99508, USA.

[54] University of Oulu, Finland & University of the Arctic.
[55] Department of Geographical Sciences, University of Maryland, College Park, MD 20742, USA.
[56] Department of Earth, Atmospheric and Planetary Sciences, Purdue University, West Lafayette, IN 47907, USA.
[57] University of Sheffield, Sheffield, UK.

*Correspondence to: snatali@whrc.org
†Authors contributed equally to this work.

Elevated warming in the Arctic, which has been amplified during the winter[1-3], greatly enhances microbial decomposition of soil organic matter and release of carbon dioxide (CO_2) from soils[4]. However, the amount of CO_2 released in winter is highly uncertain and has not been well represented by ecosystem models or by empirically-based estimates[5,6]. Here we synthesize regional *in situ* observations of CO_2 flux from arctic and boreal soils to assess current and future winter carbon losses from the pan-arctic domain. We estimate a contemporary loss of 1662 Tg C yr^{-1} from the permafrost region during the winter season (October through April). This loss is greater than the average growing season carbon uptake for this region estimated from process models (-1032 Tg C yr^{-1}). Extending model predictions to warmer conditions in 2100 indicates that winter CO_2 emissions will increase 17% under a moderate mitigation scenario—Representative Concentration Pathway (RCP) 4.5—and 41% under business-as-usual emissions scenario—RCP 8.5. Our results provide a new baseline for winter CO_2 emissions from northern terrestrial regions and show enhanced soil CO_2 loss due to winter warming may offset growing season carbon uptake under future climatic conditions.

120 Air and soil temperatures in the Arctic are increasing rapidly, with the most severe
121 climate amplification occurring in autumn and winter[1,2]. Although warmer soils decompose
122 more quickly, thus releasing more CO_2 into the atmosphere, microbial respiration is known to
123 occur even under extremely cold winter conditions (e.g., down to ~ -20°C) in the presence of
124 unfrozen microsites that can persist at sub-zero soil temperatures[7]. This production and release
125 of CO_2 in winter is expected to increase substantially as soils continue to warm and thaw under a
126 warming climate[4,8].

127 However, it remains highly uncertain how much CO_2 is currently emitted from the
128 permafrost region during winter[9] and to what magnitude these emissions might increase in the
129 future[8,10]. Many ecosystem models are not well adapted to characterize respiration from high
130 latitude soils[5] and may greatly underestimate present and future winter CO_2 emissions[6]. Given
131 the limitations in current models, lack of satellite and airborne CO_2 data for the Arctic during
132 winter[11], and gaps in spatial coverage of Arctic air monitoring networks[12], *in situ* CO_2 flux
133 observations provide the most direct insight into the state of winter CO_2 emissions across the
134 northern permafrost domain.

135 Studies of winter respiration indicate that the amount of CO_2 released during cold periods
136 depends greatly on vegetation type[13], availability of labile carbon substrates[14,15,16], non-frozen
137 soil moisture[4,7,15,17,18], microbial community composition and function[19], and snow depth[15, 20, 21].
138 However, knowledge of the influence of these drivers on the rates and patterns of winter CO_2
139 flux on a regional scale remains limited[6, 9].

140 Here we present a new compilation of *in situ* CO_2 winter flux data for the northern
141 permafrost domain (Fig. 1, Supplementary Information (SI) Table 1) to examine the drivers and
142 magnitude of winter respiration in the Arctic. We define the winter period as October through

April—months when the landscape is generally covered by snow and photosynthesis is negligible [22,23]. The dataset represents more than 100 high latitude sites and comprises more than 1,000 aggregated monthly fluxes. We examined patterns and processes driving winter CO_2 emissions and scaled fluxes to the permafrost domain using a boosted regression tree (BRT) machine learning model based on hypothesized drivers of winter CO_2 flux. Environmental and ecological drivers (e.g., vegetation type and productivity, soil moisture, and soil temperature) obtained from satellite remote sensing and reanalysis data were used to estimate regional winter CO_2 emissions for contemporary (2003-2017) climatic conditions. We estimated winter fluxes through 2100 using meteorological and carbon cycle drivers from ensembles of Earth System Model (ESM) outputs for RCP 4.5 and RCP 8.5[24].

Soil temperature had the strongest influence on winter CO_2 emissions, with fluxes measured at soil temperatures down to -20°C (Fig. 2a), in line with results from lab incubations (Fig. 2b), demonstrating that microbial respiration can occur in unfrozen microsites that persist at sub-zero bulk soil temperatures[18]. Diffusion of stored CO_2 produced during the non-frozen season may have driven some of the emissions measured in winter, but the magnitude of this contribution is unclear. Winter CO_2 emissions increased by a factor of 2.9 (95% CI = 2.1, 4.2) per 10°C soil temperature increase (i.e., Q10) for *in situ* fluxes and by a factor of 8.5 (CI= 5.0, 14.5) for CO_2 release from low temperature lab incubations. Differences between *in situ* and lab Q10s may reflect site-level differences in environmental drivers other than temperature (*in situ* and lab sites were not fully overlapping) or variation in the depth of *in situ* CO_2 production—which can occur throughout the soil profile—relative to the depth of recorded temperature, which tended to be closer to the soil surface (~ 10 cm).

Air and soil temperatures had the strongest influence on winter flux with a combined relative influence (RI) of 32%. Vegetation type (15% RI), leaf area index (LAI, 11%), tree cover (TC; 10%), and previous summer's gross primary productivity (GPP; 8.5%) also influenced winter CO_2 emissions (SI Fig. 1). Along with warmer air and soil temperatures in winter and corresponding increases in CO_2 loss, summer GPP has also been increasing across the Arctic[25]. The positive relationship between GPP and winter CO_2 emissions suggests that increased CO_2 uptake during the growing season may be offset, in part, by winter CO_2 emissions.

Another important driver of winter respiration was unfrozen water content, which is a function of soil temperature and texture, as finer textured soils contain more unfrozen water than coarse soils for a given sub-zero temperature[26]. Indirect measurements of unfrozen water availability confirm its importance: soils with low sand and high clay content, which tend to have greater unfrozen microsites, were characterized by higher CO_2 flux rates. While snow cover is a key driver of winter flux through its impact on ground temperature[27], remote sensing estimates of snow cover were not significant predictors in the model; this may be a result of high uncertainty in regional snow products or because snow depth and density, which are difficult to determine from space using currently available satellite technology[28], have a greater influence on ground temperatures than snow presence alone.

Using our model to assess winter flux for the terrestrial permafrost domain, we estimate approximately 1662 Tg C $winter^{-1}$ released under current climatic conditions (2003-2017), with a corresponding uncertainty of 813 Tg (SI Methods). There were no detected temporal trends in winter CO_2 flux during this 15-year period ($p > 0.1$), which largely reflects the lack of a significant arctic-wide trend in the reanalysis winter air or soil temperature data used as model inputs ($p > 0.1$). Although we did not observe region-wide trends during the past 15 years,

188 atmospheric CO_2 enhancements for Alaska[8] and site-level studies from Alaskan tundra[29,30]
189 showed recent increases in winter emissions, which are already shifting some tundra regions
190 from an annual carbon sink to a source.

191 Our flux estimates are twofold higher than a previous estimate derived from *in situ*
192 measurements reported in the Regional Carbon Cycle Assessment and Processes (RECCAP)
193 tundra and northern boreal domain[10], which was based on a much smaller dataset (< 20 site-years
194 for winter data). The RECCAP study reported fluxes of 24 - 41 g C m^{-2} $winter^{-1}$ from *in situ* data,
195 compared to 64 g C m^{-2} $winter^{-1}$ estimated here for the RECCAP region and 98 g C m^{-2} $winter^{-1}$
196 for the full permafrost domain (SI Fig. 2). Our estimate of winter flux agrees more closely with
197 the RECCAP atmospheric inversion estimate (27-81 g C m^{-2} $winter^{-1}$), providing some closure
198 between bottom-up and top-down assessments[6,12].

199 We then compared our permafrost region flux estimates to winter net ecosystem
200 exchange (NEE) outputs from five process-based terrestrial models and from FluxCom, a global
201 machine-learning NEE product[31]. Our winter CO_2 flux estimate was generally higher than
202 estimates from these models, which ranged from 377 Tg C $winter^{-1}$ for FluxCom and from 503 to
203 1301 Tg C for the process models (mean: 1008 Tg C $winter^{-1}$; SI Fig. 3). Similar variation in
204 carbon budget estimates from terrestrial models has been reported elsewhere for high latitude
205 regions[5] and reflects considerable differences in model parameterization of soil temperature,
206 unfrozen water, and substrate effects on CO_2 production under winter conditions. Some process-
207 based models may underestimate winter CO_2 emissions simply by erroneously shutting down
208 respiration at sub-zero soil temperatures[32] or because they are unable to capture small-scale
209 processes that influence winter flux, such as talik formation and shrub-snow interactions that are
210 more likely to be captured by *in situ* measurements.

211 Combining growing season (-687 to -1647 Tg C season^{-1}) and winter NEE derived from
212 these process models results in an estimated annual NEE of -351 to 514 Tg C yr^{-1} (-555 for
213 FluxCom; SI Table 2). Because our winter emissions estimate was higher than the process
214 models, we expect that annual CO_2 losses may also be higher. For example, if we account for
215 growing season NEE using the process model estimates, this would yield an average annual CO_2
216 emission of 646 Tg C yr^{-1} (range of 15 to 975) from the permafrost region, based on our estimate
217 of winter CO_2 flux.

218 Our assessment of future winter emissions—obtained by forcing the BRT model with
219 environmental conditions from CMIP5 ESM outputs[2]—showed significant increases in winter
220 CO_2 emissions under both climate scenarios ($p < 0.001$, Fig. 3); however, emissions were
221 substantially lower with climate mitigation in RCP 4.5 than with RCP 8.5. Compared to current
222 winter emissions (2003-2017), there was a 17% projected increase in winter CO_2 flux under RCP
223 4.5 by 2100 (to 1950 Tg C yr^{-1}) and a 41% increase under RCP 8.5 by 2100 (to 2345 Tg C yr^{-1})
224 (Fig. 4).

225 The present-day continuous permafrost zone experienced the strongest positive trend in
226 winter CO_2 emissions under both climate scenarios ($p < 0.001$); however, accounting for
227 differences in area, the largest rate of change occurred across the discontinuous zone (SI Table 3)
228 where soils have warmed rapidly and permafrost has diminished in recent years[33]. The
229 differences in projected changes in winter CO_2 emission among permafrost zones may reflect the
230 influence of latitudinal variation in environmental and ecological variables, including tree cover,
231 dominant vegetation, and soil organic matter content and composition[34].

232 Increased projected winter CO_2 emissions from our data-driven BRT model were largely
233 driven by changes in soil and air temperatures, which both increased by 0.04°C yr^{-1} under RCP

4.5, and increased by 0.08°C yr^{-1} for soil and 0.1°C yr^{-1} for air under RCP 8.5 (SI Fig. 4). Vegetation leaf area and GPP, both of which were positively related to winter CO_2 flux, also significantly increased through 2100.

From 2018 to 2100, we estimated a cumulative winter flux of 150 Pg C for RCP 4.5 and 162 Pg C for RCP 8.5. This represents an additional 15 Pg C for RCP 4.5 and 27 Pg C for RCP 8.5 emitted as a result of climate change, when compared to the estimated 135 Pg of C that would be emitted through 2100 if current (2003-2017) climatic conditions remained constant. These losses are comparable to 70% of the current permafrost-region near-surface (0-30cm) soil carbon pool[35]. These projected increases are substantially lower than projections from CMIP5 ESMs, in which winter CO_2 emissions from ecosystem respiration for the permafrost region (1753 ± 1066 Pg C yr^{-1} for 2003-2005) were projected to increase in 2100 by 37% and 86% under RCP 4.5 (2482 ± 1403 Pg C yr^{-1}) and 8.5 (3473 ± 1731 Pg C yr^{-1}), respectively (Fig. 4). Our data-driven BRT model may provide more conservative estimates because current *in situ* observations may not adequately reflect future environmental responses to substantially warmer winter conditions. However, it is also possible that the ESMs are missing stabilizing drivers and mechanisms that might provide negative feedbacks to winter CO_2 emissions. Hence, we stress the importance of addressing current uncertainties in process-model estimates of both growing season and winter CO_2 exchange. Given the data limitations during the winter, there is a particular need for long-term monitoring of winter CO_2 exchange in permafrost regions to provide key insights into processes that may enhance or mitigate change. As most of the CMIP5 models do not currently include a permafrost component, these data are critical for improving pan-arctic carbon cycle simulations.

Some of the projected winter CO_2 emissions could be offset by plant carbon uptake, which is expected to increase as plants respond favorably to warming and CO_2 fertilization[36,37]. In addition, our modeled results do not explicitly account for CO_2 uptake during the shoulder seasons (early and late winter period, e.g., October and April), which can occur, even under the snowpack[22,23,38] and which may increase with climate warming[22]. Our model projections also did not incorporate all changes expected under future climates, such as changes in permafrost distribution, delayed seasonal freeze-up, increased fire frequency, changes in snow cover and distribution, and landscape-level hydrologic changes (e.g., lake drainage).

The CO_2 emissions reported here are only part of the winter carbon budget, which also includes significant CH_4 emissions from land[17,39] and CO_2 and CH_4 emissions from inland waters[40]. Recent data-derived estimates of high-latitude terrestrial winter CH_4 emissions range from 1.6 Tg C yr^{-1} (land area > 60°N)[39] to 9 Tg C yr^{-1} for arctic tundra[17]. Similar to winter CO_2 emissions, process models significantly underestimated the fraction of annual CH_4 emissions released during the winter[39].

To reduce uncertainty in estimates of current and future emissions, we recommend increased spatial and temporal coverage and coordination and standardization of *in situ* winter measurements, improvements to regional snow density products, and development of remote sensing active sensors that can detect high resolution (< 20 km) changes in atmospheric CO_2 concentrations during periods of low to no light, which is a key constraint on efforts to monitor changes in permafrost region carbon cycling. Current rates of winter CO_2 emissions may be offsetting CO_2 uptake by vegetation across the permafrost region. Pan-arctic winter CO_2 emissions will likely increase in the near future if Arctic temperatures continue to rise; however,

278 this positive feedback on global climate can be mitigated with a reduction of global
279 anthropogenic greenhouse gas emissions.

Methods

Data overview

We compiled a dataset of *in situ* winter season (Oct-April) CO_2 emissions and potential driving variables from sites within the northern permafrost zone[41]. The synthesized dataset included 66 published studies and 21 unpublished studies (SI Table 1) conducted at 104 sites (*i.e.*, sample areas with unique geographic coordinates) and in 152 sampling locations (*i.e.*, different locations within a site as distinguished by vegetation type, landscape position*, etc.)*. Sites spanned boreal and tundra landcover classes (SI Fig. 5, SI Table 4) in continuous permafrost (n=69), discontinuous (n=24), and isolated/sporadic (n=11) permafrost zones (Fig. 1). Data were aggregated at the monthly level; however, the number of measurements per month varied among studies. The dataset included more than 1,000 site-month flux measurements. We also extracted CO_2 data from incubations of permafrost-region soils (SI Table 5) to compare their temperature response functions (Q10) with Q10 derived from the synthesized *in situ* flux data. Further details of data extraction and Q10 calculations can be found in the Supplementary Methods.

Data extraction, geospatial data

We extracted data from regional gridded geospatial products including climatological data, soil temperature and moisture, snow water equivalent, soil carbon stocks and texture, permafrost status, vegetation cover, proxies of vegetation growth and productivity (*e.g.*, enhanced vegetation index, EVI; leaf area index, LAI; gross primary productivity, GPP). See Supplementary Methods for further description and data sources. All geospatial data were re-

gridded to the National Snow and Ice Data Center Equal Area Scalable Earth (EASE) 2.0 format[42] at a 25-km spatial resolution prior to the CO_2 flux upscaling and simulations.

Boosted regression tree analysis

We used boosted regression tree analysis (BRT) to model drivers of winter CO_2 emissions and to upscale emissions to the pan-arctic region under current and future climate scenarios. The BRT model was fit in R[43] using 'gbm' package version 2.1.1[44], and using code adapted from[45]. The BRT model was fitted with the following metaparameters: Gaussian error distribution, bag-fraction (*i.e.*, proportion of data used in each iteration) of 0.5, learning rate (contribution of each tree to the final model) of 0.005, and a tree complexity (maximum level of interactions) of two. We used 10-fold cross-validation (CV) to determine the optimal number of trees to achieve minimum predictive error and to fit the final model to the data.

We used geospatial data as explanatory variables in our BRT model (See Supplementary Methods for full description of input data). We removed highly correlated variables from the models (Spearman $\rho = 0.7$), retaining the variable within each functional category (*e.g.*, air temperature) that had the highest correlation with winter flux. We further reduced the model by removing variables in reverse order of their relative influence, until further removal resulted in a 2% average increase in predictive deviance. We compared this model with one in which we included site level *in situ* data as explanatory variables. We used the geospatial model because it allowed us to upscale results and because the percent deviance (SI Table 6) and driving variables (SI Fig. 1) were similar between models.

We assessed BRT model performance using: 1. The correlation between predicted and observed values using the CV data (*i.e.*, data withheld from model fitting), hereafter referred to

as the CV correlation, and; 2. deviance explained by the model over the evaluation dataset (*i.e.,* CV data), calculated as: % deviance = (CV null deviance - CV residual deviance)/CV null deviance *100. Further details of the BRT models can be found in the Supplementary Methods.

We obtained an estimate of model uncertainty by first obtaining the average internal root mean squared error (RMSE; 0.21 g C m^{-2} d^{-1}) for the ensemble of boosted regression trees. We then made the assumption that this error applied equally to all grid cell areas within the domain. Scaling this error to the full domain (16.95×10^6 km^2) and by the total number of days for the winter (October through April) period provided us with a winter flux error of 813 Tg C.

Spatial and temporal domain for mapping

We scaled the modeled flux data to the northern permafrost land area ≥ 49° N[41], which comprises 16.95×10^6 km^2 of tundra and boreal lands (excludes glaciers, ice sheets, and barren lands; Fig. 1) with lake area removed. We defined the winter period as the months of October through April. Because the climate within this timeframe varies substantially across the permafrost zone, this month-based definition, while temporally consistent, may include some areas that are influenced by climate that would fall outside expected winter temperature ranges. Therefore, in a separate approach (presented in the Supplementary Method), we defined winter based on soil temperature, but we did not find substantial differences in regional flux budgets when using the two approaches (temperature-defined winter flux was ~ 5% higher, 1,743 Tg C, than when using the month-based winter period).

Spatial upscaling of fluxes

The BRT model was applied at a monthly time step from 2003 through 2017. For each month, the map predictions were applied to a raster stack of input predictors using the R 'dismo' package[46] for interface with the 'gbm' package and the 'raster' v2.6-7 predict function for geospatial model applications. A n.tree (# of trees) of 1,000 was selected for each model run. Output monthly mean estimates of daily CO_2 flux (g CO_2-C m^{-2} d^{-1}) were generated for each 25-km grid cell. Total pan-arctic CO_2 flux was obtained on a monthly basis by first calculating the terrestrial area for each grid cell by subtracting lake fractions (MODIS satellite product MOD44W) from each grid cell area. The fluxes were then scaled according to days per month and terrestrial area to obtain per grid cell totals.

We analyzed the pan-arctic flux data for annual temporal trends using the nonparametric Mann-Kendall test, which was run in the R 'zyp' package[47] with pre-whitening (Yue and Pilon method) to remove autocorrelation. We report Kendall's correlation coefficient, τ, to describe the strength of the time-series and Theil-Sen slope to describe trends over time.

Comparison of BRT estimates with process-based models

We compared our regional winter flux estimates to: 1) outputs from five process-based terrestrial models estimated for the northern permafrost domain: National Center for Atmospheric Research (NCAR) Community Land Model (CLM) versions 4.5 and 5; Lund-Potsdam-Jena Dynamic Global Vegetation Model (LPJ-DGVM), Wald Schnee und Landscraft version (LPJ-wsl); CARbon DAta MOdel FraMework (CARDAMOM); and the NASA SMAP Level 4 Carbon (L4C) Version 3 product; 2) estimates for the northern permafrost domain derived from FluxCom, a global gridded machine-learning net ecosystem exchange (NEE) product; and 3) four process-based terrestrial models and eight atmospheric inversion models

from the high latitude model intercomparison for the Regional Carbon Cycle Assessment and Processes (RECCAP) tundra and northern boreal domain[10]. See Supplementary Methods for further description of these models.

Projected CO_2 flux

Inputs for the BRT model of future scenarios of winter CO_2 flux were obtained from ensembles of Earth System Model (ESM) outputs from the Fifth Coupled Model Intercomparison Project (CMIP5) for RCP 4.5 and 8.5[2]. Inputs included: 1) Annual GPP; 2) mean annual summer LAI (July & August); 3) mean summer soil moisture (June, July, August); 4) mean monthly soil moisture; 5) mean monthly near-surface (2 m) air temperature; and 6) mean monthly soil temperature (layer 1) (SI Table 7). Ensemble mean RCP 4.5 and 8.5 predictor fields were bias-corrected using the delta, or perturbation method[48], based on historic ESM outputs and observed historical data and re-projected to EASE2 25 km grids.

In addition to the 0.21 g C m^{-2} d^{-1} error obtained based on the BRT model RMSE, we used the outcome from bootstrapped BRT model simulations to estimate additional, inherit prediction variability in the machine learning outcomes for current and future CO_2 emissions[49] (see Supplementary Information).

For the CMIP5 RCP 4.5 and 8.5 simulations of respiration, we used an r1i1p1 ensemble mean from 15 models (see Supplementary Information).

Data Availability: Data are archived and freely available at the ORNL Distributed Active Archive Center (DAAC). The synthesis dataset will be available at https://doi.org/10.3334/ORNLDAAC/1692. Monthly carbon flux maps (25 km, October-April, 2003-2018; 2018-2100 for RCP 4.5 and RCP 8.5) will be available at https://doi.org/10.3334/ORNLDAAC/1683.

Supplementary Information includes Supplementary Methods, Supplementary Tables 1-8, and Supplementary Figures 1-6.

Correspondence and requests for materials should be addressed to S.M.N.

Acknowledgements: This study was supported by funding from NASA's Arctic-Boreal Vulnerability Experiment (ABoVE; #NNX15AT81A to S.M.N.), with additional funding from NASA NIP (NNX17AF16G TO J.D.W.), NSF (#955713 and #1331083 to E.A.G.S.; # 1503559 to E.E.J.), the Next-Generation Ecosystem Experiments Arctic project, DOE Office of Science (E.E.J.), and funding that supported the data that were included in this synthesis.

Author contributions: S.M.N., J.D.W., and B.M.R conceived the work. B.W.A., G.C., C.T.C., H.G., E.E.J., M.M.L., S.M.L., M.L., A.M., C.M., S.M.N., F.R., B.M.R., K.S., A.S., C.C.T., Y.W., and X.X. extracted unpublished data. K.A.A, M.P.B, G.C, T.R.C, E.J.C, C.C., S.D., J.D., J.E.E., B.E., E.S.E., T.F., M.G., J.P.G., P.G., M.H., J.D.J., A.A.A.K., Y.K., L.K., K.S.L., M.L., R.M., J.M., A.M., S.M.N., W.C.O., F.W.P., N.P., W.Q., D.R., T.S., N.M.S., E.A.G.S, P.R.S.,

O.S., P.F.S., M.P.W., C.W., and D.Z. provided unpublished or raw data. L.B., A.A.B., J.D., J.S.K., Z.L., N.M., A.D.M., B.P., and Z.Z. provided modeled data/results. S.M.L., C.M., S.M.N., S.P., and J.D.W. prepared tables and figures. G.C., H.G., M.J.L., M.M.L., S.M.L, S.M.N., S.P., B.M.R., P.F.S., and J.D.W. performed statistical analyses, including BRT modeling. S.P., B.M.R., and J.W. led the BRT upscaling or projection analyses. All authors contributed to data interpretation and preparation of manuscript text.

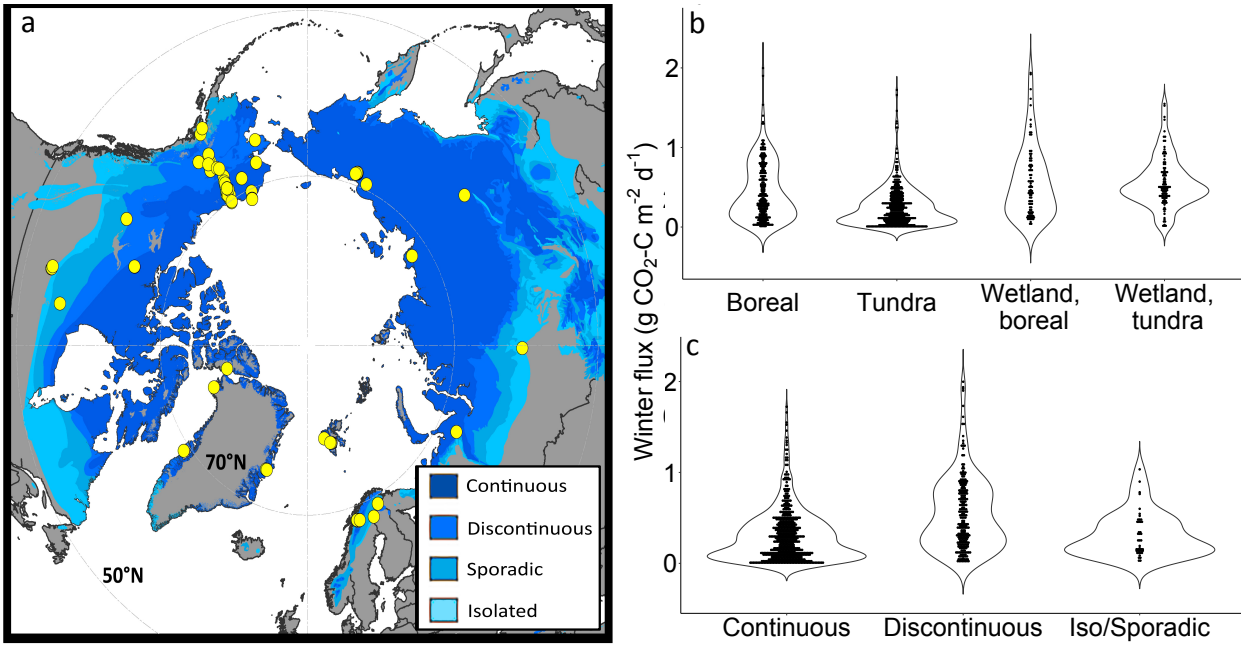

Fig. 1. Distribution of *in situ* data included in this winter CO_2 flux synthesis. (a) Locations of *in situ* winter CO_2 flux data (yellow circles) in this synthesis included (b) upland and wetland sites in boreal and tundra biomes located (c) within the northern permafrost region[41]. Violin plots (b,c) depict magnitude and distribution density (width; dots are monthly aggregated data) of *in situ* data used in our machine-learning model.

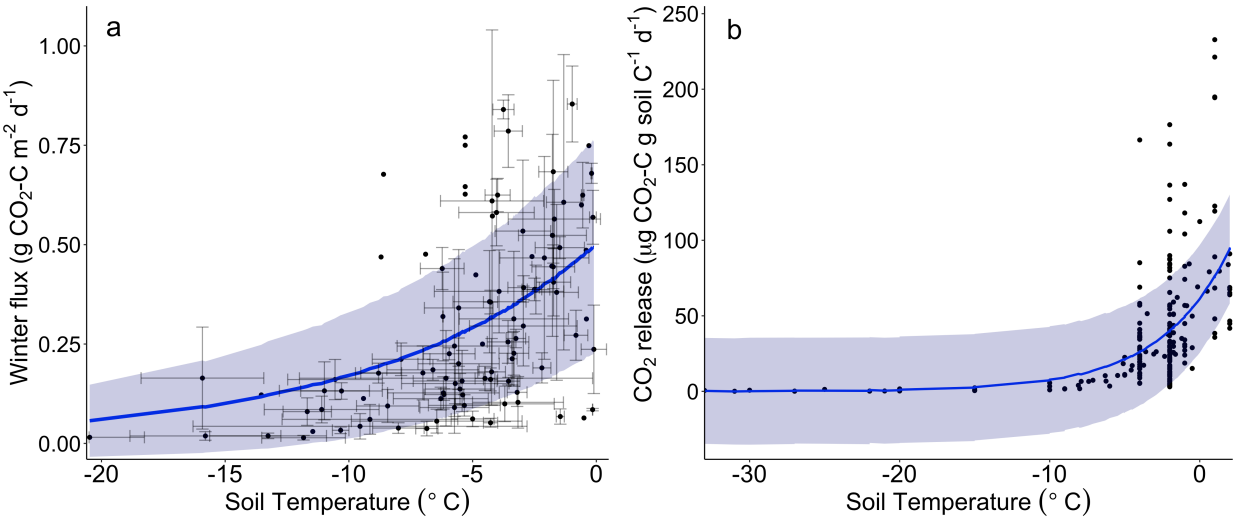

Fig. 2. Effect of soil temperature on CO_2 release from soils. (a) Relationships between *in situ* soil temperature (~ 10 cm average depth) and CO_2 fluxes and (b) temperature and CO_2 released from lab incubations. Shading represents the standard deviation of an exponential model, which, for *in situ* fluxes, was fit to mean CO_2 flux from each sample location (symbols shown with standard error). Note that the different soil temperature scales between panels reflect data ranges.

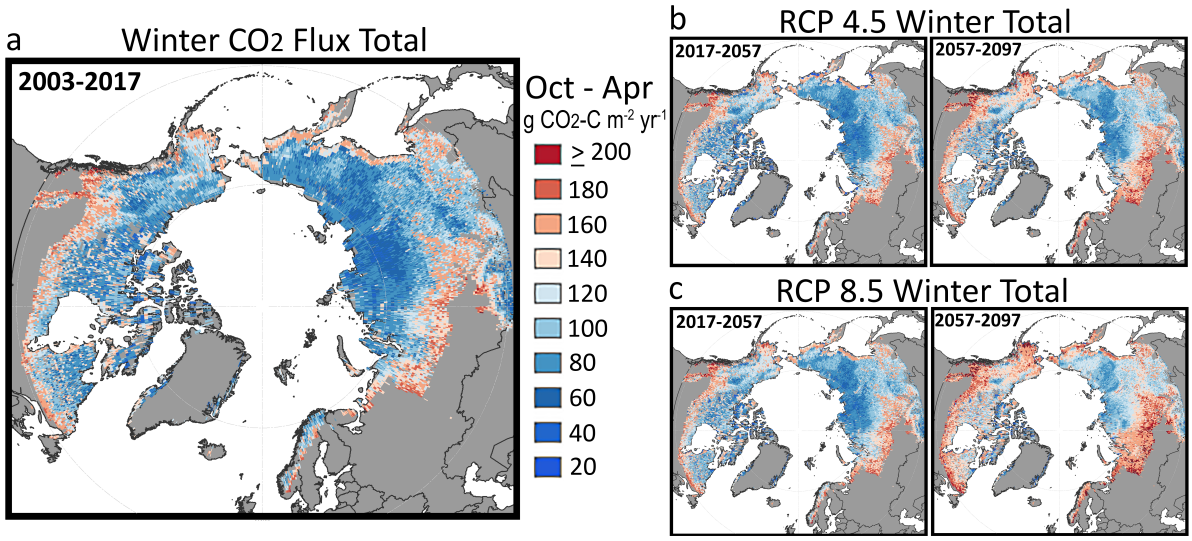

436

437 **Fig. 3. Pan-Arctic winter CO_2 emissions under current and future climate scenarios.** (a)

438 Average annual winter (October - April) CO_2 emissions estimated for the permafrost region for

439 the baseline years 2003-2017. Cumulative winter CO_2 fluxes under (b) RCP 4.5 and (c) RCP 8.5

440 scenarios over an 80-year period (2017-2057 and 2057-2097). Fluxes are reported on an annual

441 basis (g CO_2-C m^{-2} yr^{-1}).

442

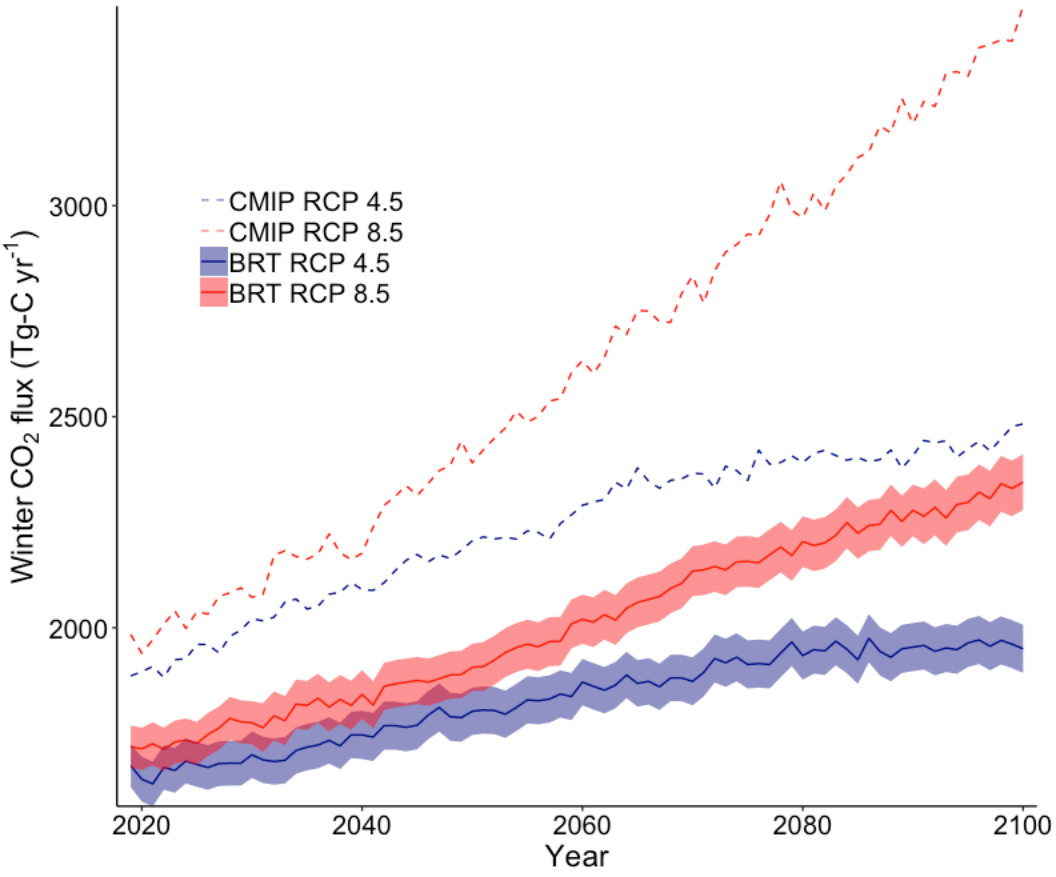

Fig. 4. Projected annual CO_2 emissions during the winter for the northern permafrost region. Solid lines represent BRT modeled results through 2100 under RCP 4.5 (red solid line) and RCP 8.5 (blue solid line), with bootstrapped 95% confidence intervals indicated by shading. For reference, CMIP5 ensemble respiration for RCP 4.5 and 8.5 are also shown (dashed lines).

References

1 Huang, J. Recently amplified arctic warming has contributed to a continual global warming trend. *Nat. Clim. Change* **7**, 875-879 (2017).

2 Koenigk, T. et. al. Arctic climate change in 21st century CMIP5 simulations with EC-Earth. *Clim. Dyn.* **40**, 2719-2743 (2013).

3 Cohen, J., Screen, J.A., Furtado, J.C., Barlow, M., et al. Recent Arctic amplification and extreme mid-latitude weather. *Nature Geosci.* **7**, 627-637 (2014).

4 Schadel, C., Bader, M.K-F., Schuur, E.A.G., Biasi, C., Bracho, R. et al. Potential carbon emissions dominated by carbon dioxide from thawed permafrost soils. *Nat. Clim. Change* **6**, 950-953 (2016).

5 Fisher, J. B. et. al. Carbon cycle uncertainty in the Alaskan Arctic. *Biogeosciences* **11**, 4271-4288 (2014).

6 Commane, R., Lindaas, J., Benmergui, J., Luus, K.A., et al. Carbon dioxide sources from Alaska driven by increasing early winter respiration from Arctic tundra. *Proc. Natl. Acad. Sci.* **114**, 5361-5366 (2017).

7 Elberling, B., Brandt, K.K. Uncoupling of microbial CO_2 production and release in frozen soil and its implications for field studies of arctic C cycling. *Soil Biol. Biogeochem.* **35**, 263-272 (2003).

8 Schuur, E. A. G., McGuire, A.D., Schadel, C., Grosse, G., et al. Climate change and the permafrost carbon feedback. *Nature* **520**, 171-179 (2015).

9 Belshe, E. F., Schuur, E.A.G., Bolker, B.M. Tundra ecosystems observed to be CO_2 sources due to differential amplification of the carbon cycle. *Ecology Lett.* **16**, 1307-1315 (2013).

10 McGuire, A. D. et. al. An assessment of the carbon balance of Arctic tundra: Comparisons among observations, process models, and atmospheric inversions. *Biogeosciences* **9**, 3185–3204 (2012).

11 Schimel, D., Pavlick, R., Fisher, J.B., Asner, G.P. et al. Observing terrestrial ecossytems and the carbon cycle from space. *Glob.Change Biol.* **21**, 1762-1776 (2014).

12 Parazoo, N., Commane, R., Wofsy, S.C., Koven, C.D. Detecting regional patterns of changing CO2 flux in Alaska. *Proc. Natl. Acad. Sci.* **113**, 7733-7738 (2016).

13 Grogan, P. Cold season respiration across a Low Arctic landscape: The influence of vegetation type, snow depth, and interannual climatic variation. *Arctic, Antarct. Alp. Res.* **44**, 446–456 (2012).

14 Michaelson, G. J., Ping, C.L. Soil organic carbon and CO_2 respiration at subzero temperature in soils of Arctic Alaska. *J.G.R. Atmos.* **108** (2005).

15 Rogers, M. C., Sullivan, P.F., Welker, J.M. Evidence of nonlinearity in the response of net ecosystem CO_2 exchange to increasing levels of winter snow depth in the high Arctic of Northwestern Greenland. *Arct. Antarc. Alpine Res.* **43**, 95-106 (2011).

16 Wang, T., Ciais, P., Piao, S.L., Ottle, C., et al. Controls on winter ecosystem respiration in temperate and boreal ecosystems. *Biogeosciences* **8**, 2009-2025 (2011).

17 Zona, D., Gioli, B., Commane, R., Lindaas, J., et al. Cold season emissions dominate the Arctic tundra methane budget. *Proc. Natl. Acad. Sci.* **113**, 40-45 (2016).

18 Schaefer, K. J., et al. A parameterization of respiration in frozen soils based on substrate availability. *Biogeosciences* **13**, 1991–2001 (2016).

19 Monson, R., Lipson, D., Burns, S.P., Turnipseed, A.A., et al. Winter forest soil respiration controlled by climate and microbial community composition. *Nature* **439**, 711-714 (2006).

20 Welker, J. M., Fahnestock, J.T., Jones, M.H. Annual CO_2 flux in dry and moist arctic tundra: field responses to increases in summer temperatures and winter snow depth. . *Clim. Chan* **44**, 139-150 (2000).

21 Natali, S. M., Schuur, E.A.G., Trucco, C., Hicks Pries, C.E., et al. Effects of experimental warming of air, soil and permafrost on carbon balance in Alaskan tundra. *Glob. Chan. Biol.* **17**, 1394-1407 (2011).

22 Webb, E. E., et. al. Increased wintertime CO_2 loss as a result of sustained tundra warming. *Biogeosciences* **121**, 1-17 (2016).

23 Christiansen, C. T., Schmidt, N. M. & Michelsen, A. High Arctic dry heath CO_2 exchange during the early cold season. *Ecosystems* **15**, 1083-1092 (2012).

24 Knutti, R., Masson, D. & Gettelman, A. Climate model genealogy: Generation CMIP5 and how we got there. *Geophys. Res. Lett.* **40**, 1194–1199 (2013).

25 Forkel, M., et. al. Enhanced seasonal CO_2 exchange caused by amplified plant productivity in northern ecosystems. *Science* **351**, 696-699 (2016).

26 Tucker, C. Reduction of air- and liquid water-filled soil pore space with freezing explains high temperature sensitivity of soil respiration below 0 degrees C. *Soil Biol. Biochem.* **78**, 90–96 (2014).

27 Huang, Y., Jiang, J., Ma, S., Ricciuto, D., Hanson, P.J., Luo, Y. Soil thermal dynamics, snow cover, and frozen depth under five temperature treatments in an ombrotrophic bog: constrained forecast with data assimilation. *J.G.R. Biogeosci.* **122**, 2046-2063 (2017).

28 Witze, A. Snow-sensing fleet to unlock water's icy secrets. *Nature* **7**, 1, doi:doi: 10.1038/532017a (2016).

29 Natali, S. M., Schuur, E.A.G., Mauritz, M., Schade, J.D., et al. Permafrost thaw and soil moisture driving CO_2 and CH_4 release from upland tundra. *J.G.R. Biogeosci.* **120**, 525-537 (2015).

30 Euskirchen, E. S., Bret-Harte, M. S., Shaver, G. R., Edgar, C. W., Romanovsky, V. E. Long-term release of carbon dioxide from arctic tundra ecosystems in Alaska. . *Ecosystems* **20**, 960–974 (2017).

31 Tramontana, G., et. al. Predicting carbon dioxide and energy fluxes across global FLUXNET sites with regression algorithms. *Biogeosciences* **13**, 4291–4313 (2016).

32 Koven, C. D., et. al. Permafrost carbon-climate feedbacks accelerate global warming. *Proc. Natl. Acad. Sci.* **108**, 14769–14774 (2011).

33 Slater, A. G., & Lawrence, D.M. Diagnosing present and future permafrost from climate models. . *J. Climate* **26**, 5608-5623 (2013).

34 Vanhala, P., K. Karhu, M. Tuomi, K. Bjorklof, H. Fritze, J. Liski. Temperature sensitivity of soil organic matter decomposition in southern and northern areas of the boreal forest zone. *Soil Biol. Biochem.* **40**, 1758-1764 (2008).

35 Hugelius, G. e. a. Estimated stocks of circumpolar permafrost carbon with quantified uncertainty ranges and identified data gaps. . *Biogeosciences* **11**, 6573–6593 (2014).

36 McGuire, A. D., et. al. Dependence of the evolution of carbon dynamics in the northern permafrost region on the trajectory of climate change. *Proc. Natl. Acad. Sci.*, doi:doi:10.1073/pnas.1719903115 (2018).

37 Qian, H., Joseph, R., Zeng, N. Enhanced terrestrial carbon uptake in the Northern High Latitudes in the 21st century from the Coupled Carbon Climate Model Intercomparison Project model projections. *Glob. Chan. Biol.* **16**, 641-656, doi:10.1111/j.1365-2486.2009.01989.x.
38 Starr, G. O., et. al. Photosynthesis of Arctic evergreens under snow: Implications for tundra ecosystem carbon balance. *Ecology* **84**, 1415-1420 (2003).
39 Treat, C. C., Bloom, A. A. & Marushchak, M. E. Nongrowing season methane emissions–a significant component of annual emissions across northern ecosystems. . *Glob. Chang. Biol.* **24**, 3331–3343 (2018).

Methods References

40 Walter Anthony, K., et. al. 21st-century modeled permafrost carbon emissions accelerated by abrupt thaw beneath lakes. *Nat. Commun.* **9** (2018).
41 Brown, J., Ferrians, O., Heginbottom, J. & Melnikov, E. Circum-Arctic map of permafrost and ground-ice conditions, version 2. (2002).
42 Brodzik, M. J., Billingsley, B., Haran, T., Raup, B. & Savoie, M. H. EASE-Grid 2.0: Incremental but significant improvements for Earth-gridded data sets. *ISPRS Int. J. Geo-Information* **1**, 32-45 (2012).
43 Team., R. C. R: A language and environment for statistical computing. (2016).
44 Ridgeway, G. Generalized Boosted Models: A guide to the gbm package. 1-12 (2007).
45 Elith, J., Leathwick, J. R. & Hastie, T. A working guide to boosted regression trees. *J. Anim. Ecol.*, 802-813 (2008).
46 Hijmans, R. J., Phillips, S., Leathwick, J. & Elith, J. . R "dismo" package. (2017).
47 Bronaugh, D. W. R "zyp" trends package. (2017).
48 Rogers, B. M., et. al. Impacts of climate change on fire regimes and carbon stocks of the U.S. Pacific Northwest. *J. Geophys. Res. Biogeosciences* **116** (2011).
49 Leathwick, J. R., Elith, J., Francis, M. P., Hastie, T. & Taylor, P. Variation in demersal fish species richness in the oceans surrounding New Zealand: An analysis using boosted regression trees. *Mar. Ecol. Prog. Ser.* **321**, 267–281 (2006).